Rapid Selective Detection of Ascorbic Acid Using Graphene-Based Microfluidic Platform

Goran M. Stojanović, *Member, IEEE*, Tijana Kojić, Mitar Simić, *Member, IEEE*, Aleksandra Jovanović-Galović, Bojan Pavlović, Amaia Zurutuza, Luca Anzi, and Roman Sordan

***Abstract*—In this paper, we present a compact microfluidic platform for selective detection of ascorbic acid. The microfluidic chip was fabricated by xurography technique with microfluidic channel placed between the silver electrodes. To increase the conductivity of the platform and enhance electron transfer process, a graphene sheet was deposited in the gap between the electrodes. The suspension of tablets with ascorbic acid and a mixture of ascorbic acid and isomalt, a sugar substitute, were injected in the microfluidic channel. Measuring electrical parameters at the silver contacts, it was possible to successfully differentiate ascorbic acid from isomalt. The sensing mechanism of the developed microfluidic platform is based on the increase of the overall conductivity with the increase of the concentration of ascorbic acid, resulting in the decrease of the resistive parameters and increase of the capacitive parameters of the proposed equivalent electrical circuit. The addition of graphene was found to improve the response linearity by 5.28% and lower the limit of detection and quantification by 12%, compared to the reference structure without graphene.**

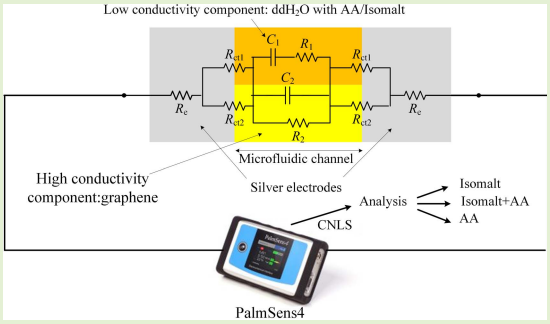

***Index Terms*—Microfluidics, graphene, ascorbic acid, impedance spectroscopy.**

I. Introduction

NUTRIONAL supplements have been increasingly popular in recent decades. The emerging field of "nutraceuticals" [1] emphasizes the importance of nutrition and dietary supplements, not only as an essential factor for prevention of diseases and maintaining good health but also as a way to treat various pathological conditions – alone or in combination with drugs. Ascorbic acid (AA) is a natural organic acid that is widely present in fruits. The AA content is also considered as an indicator of the freshness of the fruits. Since the human body does not produce AA, it is essential to have adequate AA intake through food, drugs or dietary supplements (recommended dietary allowance is ∼120 mg/day). AA can be added in pharmaceutical formulations in order to prevent or cure some diseases, e.g., common cold and hypohemia [2].

The conventional techniques for the detection of AA are chromatography [3], spectrophotometry [4], and fluorometry [5]. It has been demonstrated that the liquid chromatography can also be coupled with electrochemical methods to determine the amount of AA in real samples such as oranges and apples, pharmaceutical preparations, and human blood serum [6]. Some recent approaches for AA detection are based on optical fiber sensors [7], [8]. A Ge-doped photosensitive optical fiber demonstrated a wide linear range of detection from 1 μM to 1 mM [7]. Moreover, a localized surface plasmon resonance based AA sensor exhibited good chemical and mechanical behavior [8]. Despite the fact that optical-based approaches are promising in terms of the sensitivity

Manuscript received April 13, 2021; accepted April 29, 2021. Date of publication May 10, 2021; date of current version July 30, 2021. This work was supported in part by the EU H2020 Research and Innovation Program by the Marie Skłodowska-Curie Grant through the innovative bio-inspired sensors and microfluidic devices for saliva-based theranostics of oral and systemic diseases (SALSETH) under Agreement 872370 and in part by the EU H2020 Graphene Flagship Core 3 under Grant 881603. The associate editor coordinating the review of this article and approving it for publication was Dr. Giuseppe Barillaro. *(Corresponding author: Mitar Simić.)*

Goran M. Stojanović, Tijana Kojić, and Mitar Simić are with the Faculty of Technical Sciences, University of Novi Sad, 21000 Novi Sad, Serbia (e-mail: sgoran@uns.ac.rs; kojictijana@uns.ac.rs; mitar.simic@uns.ac.rs).

Aleksandra Jovanović-Galović is with the Faculty of Pharmacy, University of Novi Sad, 21000 Novi Sad, Serbia (e-mail: aleksandra.jovanovic@faculty-pharmacy.com).

Bojan Pavlović is with PhytoNet AG Company, 21000 Novi Sad, Serbia (e-mail: bpavlovic@phytonet.com).

Amaia Zurutuza is with Graphenea, 20018 San Sebastián, Spain (e-mail: a.zurutuza@graphenea.com).

Luca Anzi and Roman Sordan are with the L-NESS, Department of Physics, Politecnico di Milano, 20133 Milan, Italy (e-mail: luca.anzi@polimi.it; roman.sordan@polimi.it).

Digital Object Identifier 10.1109/JSEN.2021.3078692

and reliability in AA detection, these methods require costly equipment such as fusion splicers and spectrophotometers, trained personnel, and time-consuming procedures for sample preparation, which make them not optimized for *in-situ* applications outside the laboratory.

Electrical impedance spectroscopy (EIS) is a very versatile method for investigating electrode-solution interfaces and processes at the electrodes immersed in solutions of interest. EIS is non-invasive and allows to associate changes of solution properties (e.g., conductivity, permeability, and permittivity) to the changes of the measured impedance between the electrodes. Therefore, changes in a solution can be observed by a nondestructive characterization process. Additional advantage of EIS is an economic aspect as reliable impedance measurement devices can be portable and adopted for specific applications in terms of the measurement range. Interfacing of EIS with various sensors has been reported by many authors, including an immunoassay for detection of carcinoembryonic antigen [9]–[11], dissolved H_2S [12], prostate-specific antigen [13], Hg^{2+} [14], and biosensing of Cu^{2+} in aqueous solutions [15].

Recently, the application of microfluidic technologies in detection systems become very attractive choice for the manufacturing of sensor platforms [16]. Main features of microfluidic platforms are small size, ability to analyze small quantity of samples, and perform multi-step analysis with non-turbulent flow of fluids [16]. Moreover, microfluidic technology offers integration of various components in a single platform [16]. Therefore, flexibility, rapid analysis, low fabrication costs, ease of implementation and disposability promote microfluidic technology to a very popular solution in biochemical sensing [17]–[36].

AA is soluble in water, allowing the application of food microfluidics. Polydimethylsiloxane-based microfluidic chips/sensors have been coupled with ultraviolet–visible (UV/vis) spectroscopy for the quantification of AA [17], [18]. A microfluidic platform based on screen-printed carbon electrodes for the detection of dopamine and AA using chronoamperometric method has been reported [19]. In addition, microfluidic chips can be based on paper, as an inexpensive substrate material, for the realization of analytical devices with good performances. Testing of a microfluidic paper-based prototype for detection and separation of AA and uric acids has been demonstrated [20]. The concentration of AA has been determined in the commercial tablets of C vitamin by means of a device based on paper and graphite pencil [21]. An electrochemical sensor based on flexible graphite paper for determination of AA, dopamine and uric acid has been fabricated [22].

With the fast development of nanotechnology and discovery of new nanomaterials, such as carbon nanotubes (CNTs) and graphene, new sensing devices were realized for prostate-specific antigen [23], visual screening of H_2S [24], gas biosensors [25] and AA detection [26]. CNTs, with their excellent electrical and mechanical properties, have been used as a sensor for AA [27] or for improving AA detection by the electrochemical methods [28]. Thanks to its exceptional electronic properties and two-dimensional structure, graphene has also been used as a building block in many biosensing applications. The graphene/CuPc/PANI nanocomposite structure has been manufactured by electrolytic exfoliation technique for the determination of AA and investigation of its electrochemical characteristics [29], [30]. The complete measurement system based on the complex structure of the magnetic beads-ascorbate oxidase/graphene oxide/indium gallium zinc oxide/aluminium and the microfluidic device has been developed and tested as a biosensor of AA [31]. An AA sensor validated by means of a commercial vitamin C supplement, applying a structure based on pyrolysed photoresist films and graphene nano-sheets, has been demonstrated [32]. The graphene doped carbon paste electrode has been employed for ensuring good electrochemical current responses for the electrocatalytic oxidation of AA [33]. The simultaneous determination of AA, dopamine, and uric acid has been demonstrated, applying a sensor realized from pristine graphene [34]. The same application has been reported using a nanocomposite of graphene and size-selected Pt nanoparticles [35]. A sensor based on NiO nanoparticles and graphene composite film for the determination of AA in the presence of folic acid has been demonstrated [36].

Therefore, there is a need for microfluidic sensing devices for rapid separation and determination of dietary supplements. Particularly, it is of great importance to have an accurate method and device for AA detection. Considering that commercially available vitamin C supplements also contain a significant amount of sweeteners, it is crucial to differentiate AA from isomalt, a widely applied sugar substitute. Therefore, a combination of EIS, microfluidic technologies and graphene presents a viable route for AA detection and observation in the presence of isomalt.

Here, we demonstrate a microfluidic platform for the efficient detection of AA by measuring electrical parameters between Ag electrodes. The electrodes were inkjet printed with Ag ink to minimize the electrical resistance. Realization of the platform with polyvinylchloride (PVC) thermosensitive foils provided robustness of the platform. The proposed platform uses a chemically unmodified graphene layer in the gap between the Ag electrodes ensuring a cost-effective and straightforward fabrication process. We used graphene to enhance the sensitivity of the impedance-based sensing platform which has a small active surface area [23]–[25]. Graphene is an excellent candidate for biochemical sensing because it has very good physical properties, such as high thermal conductivity (3000 $Wm^{-1}K$), high surface-to-volume ratio (2600 m^2g^{-1}), high carrier mobility (15000 $cm^2V^{-1}s^{-1}$) and exceptional thermal stability [25]. Based on the simple impedance measurements and fitting the electrical response of the sensor to the proposed equivalent electrical circuit, the microfluidic platform enabled a quick and cost-effective determination of the AA concentration in the food supplement tablets.

II. Materials and Methods

A. Design of Microfluidic Platform and Materials

The proposed microfluidic platform was fabricated as a multi-layered structure composed of PVC transparent foils, as shown in Fig. 1(a). On the bottom PVC foil, which has

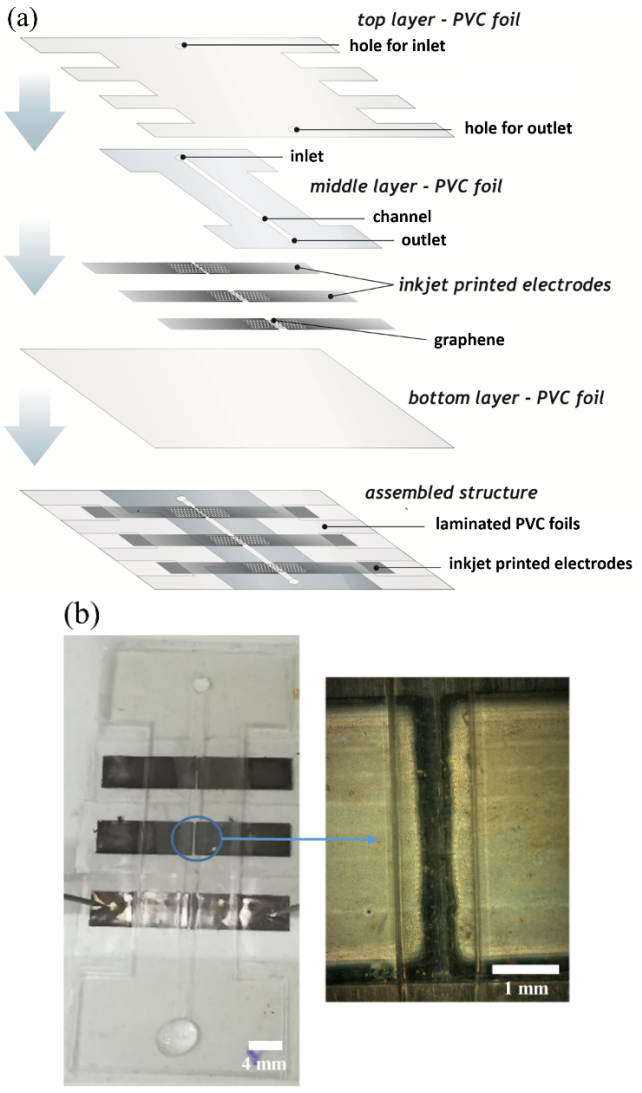

Fig. 1. (a) Design of the microfluidic platform, (b) A photo of the fabricated microfluidic platform and a zoomed-in part of the gap between the electrodes.

the role of a substrate, the three pairs of Ag electrodes were inkjet printed, ensuring the reliability of the entire device. The Ag-electrodes were used for several reasons: (a) Ag has the highest electrical conductivity among the conventional conductive materials, (b) Ag-ink is the most often used with inkjet printers, such as Dimatix inkjet printer DMP-3000, applied in this study, (c) Ag-electrodes provide reliable terminals for connections to the external electronics, and (d) graphene has an affinity to create a good electrical contact with Ag [37]. The lateral dimensions of the electrodes were 10 mm $\times$ 4 mm, and their thickness was $\sim$250 nm. There is a short gap (length $\sim$0.3 mm) between the electrodes (Fig. 1(b)). Graphene was grown by chemical vapor deposition on a Cu foil and transferred by a wet process on top of the Ag electrodes, providing an electrical connection between the electrodes. TEM image of the used graphene is shown in Fig. 2. In the middle layer, a microfluidic channel was curved using a cutting plotter. At the top layer, PVC foil was used, as a cost-effective material, with an inlet and outlet for the tested fluid. The three PVC layers were laminated together at 130 °C

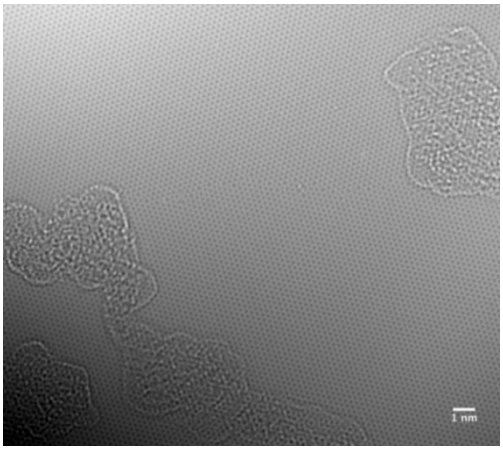

Fig. 2. TEM image of the used graphene.

to obtain a compact portable microfluidic platform, which is easy to handle and manipulate. The fabricated microfluidic chip is depicted in Fig. 1(b). The overall chip dimensions were 2.5 cm $\times$ 5.5 cm.

B. Fabrication and Characterization Methods

The deposition material printer DMP-3000 (Dimatix) was used to print electrodes on PVC foil (80 μm thick, MBL 80MIC A4 hot lamination foil, Minoan Binding Laminating d.o.o. Serbia). Inkjet printing parameters were: the minimum droplet diameter was 36 μm and the spacing between drops was 18 μm. The inkjet printing process, using Dimatix printer, was optimized to achieve a stable stream of droplets without the "satellite" drops. The latter are a byproduct of the droplet formation and could short circuit the printed electrodes. The quality of the printed continuous conductive lines depends on the droplet diameter and spacing between the drops. These two parameters determine the degree of the overlap between the droplets. They were optimized based on our previous results [38], [39] in order to obtain conductive lines with good conductivity and straight edges. We found that the droplet diameter should be $<$36 μm to avoid irregular line edges and spacing $<$18 μm to avoid gaps in the conductive lines.

Graphene was wet-transferred in the gap between the Ag electrodes (printed using Ag nanoparticle ink). Microfluidic channel was created by a xurography technique. Namely, the cutting plotter (CE6000-60 PLUS, Graphtec America, Inc., USA) was used for engraving straight line (with a width of 1 mm and length of 4 cm) and holes (diameter of 2 mm) in the PVC foil, for the inlet and outlet. For engraving, a cutting blade with a 45° angled tip was used. A hot laminator was used to laminate the individual layers into a single compact structure. Electrochemical measurements were performed using PalmSens4 instrument at room temperature. The PalmSens4 was a computer-controlled via a Bluetooth link, and software tool PS Trace 5.8 was used for performing measurements and exporting the measured data.

C. Preparation of the Testing Samples

Tablets were prepared by PhytoNet AG [40], in accordance with good manufacturing practice. The first group of tablets

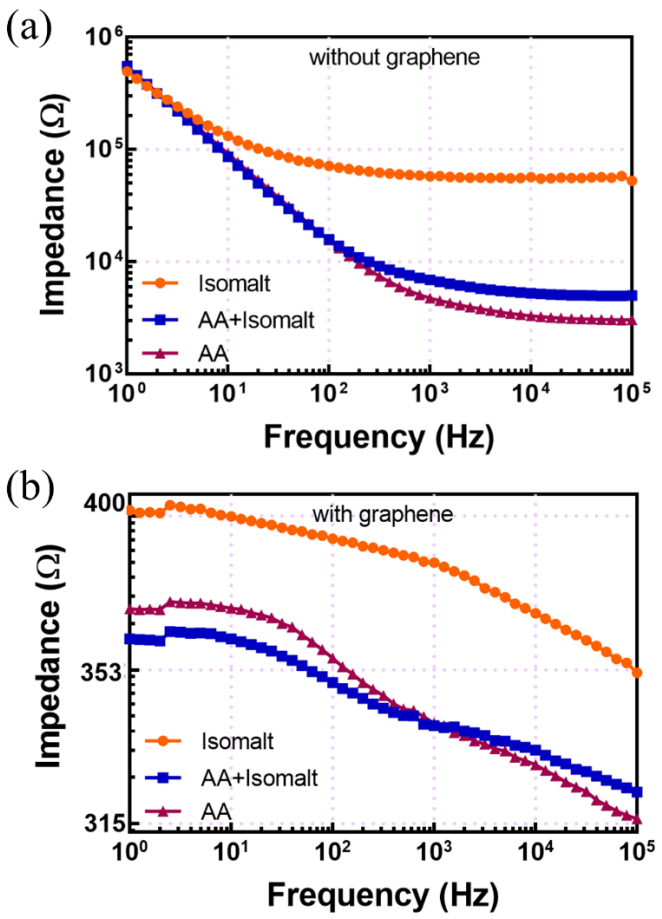

Fig. 3. Impedance as a function of frequency for a sample (a) without graphene and (b) with graphene.

comprised pure isomalt which is water-soluble and cannot be bound on the active substance (AA in this case). The second group of tablets comprised pure AA. The third group of tablets comprised a mixture of 50% of isomalt and 50% of AA. For the electrochemical measurements, the tablets were dissolved in 5 ml of double-distilled water (ddH_2O), and filtered through a 0.22 μm syringe filter ensuring bacteria-free samples. This procedure is known as sterilization by filtration. Due to the pore size of the used filters, all particles larger than 0.22 μm in size, including bacteria [41], [42], were trapped by the filter. Each step was performed in sterile tubes and syringes and handled using sterile gloves. The microfluidic channel was cleaned with deionized water after each measurement.

III. Results and Discussion

A. Electrochemical Impedance Spectroscopic Analysis

We implemented the impedance spectroscopy analysis to characterize the samples without and with graphene between the Ag electrodes. The PalmSens4 instrument was setup in two-electrode configuration, and frequency range from 1 Hz to 100 kHz was covered with 50 logarithmically spaced points. Measured impedance magnitude (or "impedance" for short) as a function of frequency is shown in Fig. 3.

TABLE I
Quantitative Study of Sensing Performances

	R^2	|LOD|	|LOQ|
Without graphene	0.777	125.01	378.82
With graphene	0.818	110.03	333.43

In the structure without graphene, the smallest impedance was obtained with pure AA inside the channel. A mixture of 50 % AA + 50 % isomalt had larger impedance, while the largest impedance was obtained with pure isomalt. The measured impedance was in order of tens/hundreds of kΩ which was dominated by the low conductivity medium (ddH_2O) between the electrodes. In general, pure ddH_2O is very similar to an insulator, but it has some low finite conductivity. Such low conductivity medium can be modelled by a series RC network [43]. Values of the network elements mostly depend on ion concentration, mobility, and size of the particles of active substance. A typical plot of the electrical impedance of the series RC network versus frequency (with logarithmic scale on the both axes) is linear at low frequencies and has a plateau at high frequencies [43]. It exhibits a very similar trend as obtained in Fig. 3(a).

An addition of a graphene layer, in the gap between the Ag electrodes of the microfluidic platform, did not change the relative order of the impedances: the structure with AA inside the channel had the lowest impedance, while the structure with isomalt had the highest impedance (Fig. 3(b)). However, the addition of graphene resulted in a significant decrease of the impedance compared to the microfluidic platform without graphene. For example, at a frequency of 10 kHz, the impedance without graphene for isomalt, AA + isomalt, and AA was 56.6 kΩ, 5.22 kΩ, and 3.31 kΩ, respectively. At the same frequency, the measured impedance with graphene was 368.6 Ω, 332.8 Ω and 329.2 Ω, for isomalt, AA + isomalt and AA, respectively. The advantages of the lower impedance of the microfluidic platform with graphene are easier electron transfer and interfacing with the measurement unit.

Fig. 4 shows calibration curves for chips without and with graphene at the frequency of 10 kHz. The graphs also depict the corresponding linear fits.

In order to quantitatively compare performances of the investigated microfluidic structures with and without graphene, the coefficient of linearity (R^2), limit of detection (LOD), and limit of quantification (LOQ) were calculated. The LOD (Table I) was calculated as 3.3· *Ste*/*b* and LOQ as 10· *Ste*/*b*, where *Ste* is the standard error from regression statistics and *b* is the slope coefficient of the calibration curve of the linear regression lines. The confidence interval of 95% was implemented.

It can be seen in Table I that the chip with graphene has a better coefficient of linearity (by 5.2 %), and lower LOD and LOQ (by 12%) compared to the chip without graphene. Therefore, in addition to reducing the impedance of the sensor, the introduction of graphene improved the linearity of the response and enabled lower levels of detection

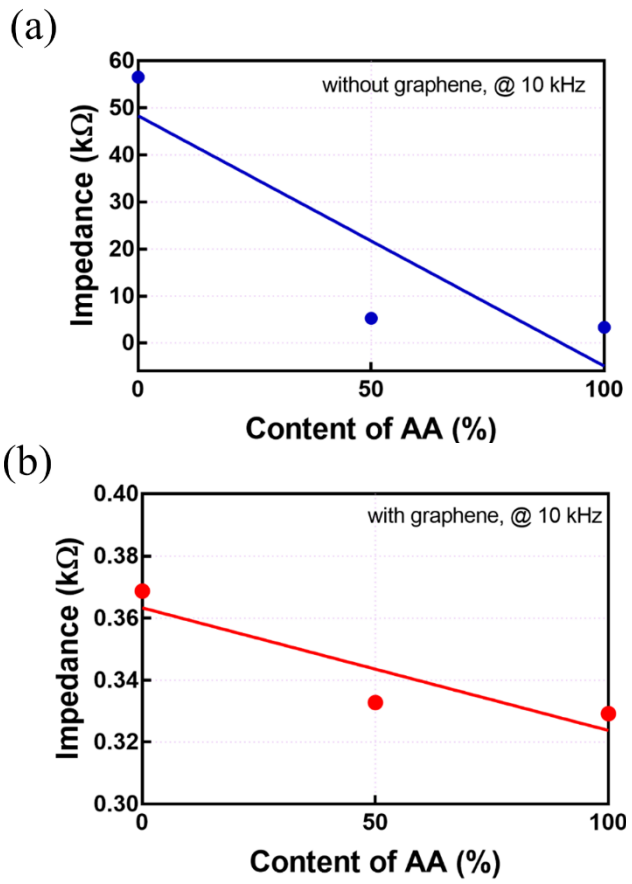

Fig. 4. Calibration curves for chips: (a) without graphene, (b) with graphene. The impedances were measured at a frequency of 10 kHz.

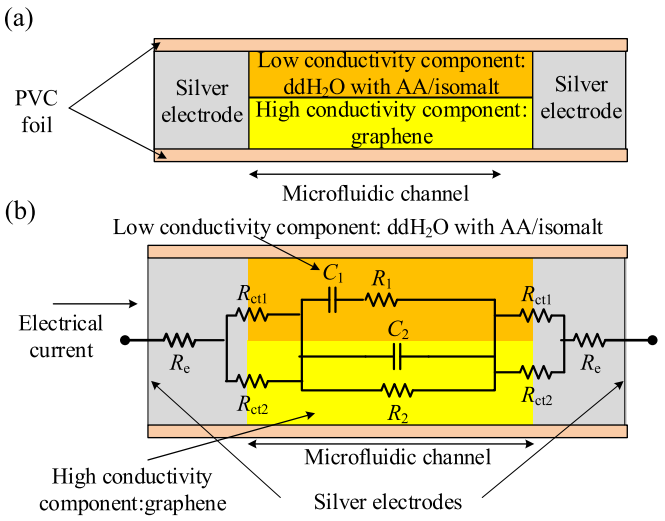

Fig. 5. (a) Resulting structure with low conductivity phase on the top of the graphene layer (not in scale), (b) lumped electrical model of the fabricated sensors.

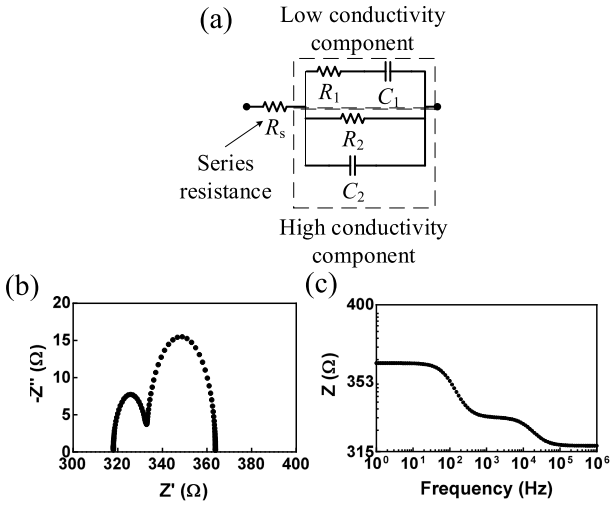

Fig. 6. (a) Proposed equivalent circuit. (b) Typical Nyquist plot of a proposed equivalent electrical circuit. Z' and Z" are the real and imaginary part of the complex impedance. (c) Corresponding impedance plot versus frequency (logarithmic scale on both axes).

and quantification. Obtained characteristics justify the incorporation of graphene in our microfluidic platform.

The reproducibility of the proposed sensing platform was evaluated by fabricating samples with three pairs of Ag electrodes on the same substrate. The same experiments were performed on all three pairs of contacts obtaining similar results with a satisfactory relative standard deviation of 4.17%. The platform was also reusable because two consecutive sets of experiments yielded the same results if the microfluidic channel was rinsed with distilled water between the experiments. Using one pair of electrodes, it was possible to perform many measurements due to the excellent mechanical properties of the graphene layer and unnecessity to apply high pressure on the injected solution in the microfluidic channel.

A significantly smaller impedance of the platform with graphene was attributed to the high conductivity of graphene (1738 S/m, equivalent to a resistivity of 0.0575 Ω·cm) [44]. The transferred graphene layer established an additional low-resistance current path between the electrodes. Thus, the resulting structure had two phases: low conductivity (ddH_2O with AA/isomalt) and high conductivity (graphene) phase, as illustrated in Fig. 5(a). Fig. 5(b) depicts the electrical model of the fabricated sensor.

The low conductivity phase can be modelled as a series connection of a resistor (R_1) and capacitor (C_1), as shown in Fig. 6(a). This can be understood from Fig. 3(a), where impedance change with frequency is presented for the system without graphene. Resistance R_1 is the solution resistance, while C_1 models dielectric properties of the solution. The high conductivity phase is composed of graphene layer, and it is modelled as a resistor (R_2) and capacitor (C_2) connected in parallel [45], [46]. R_2 is the resistance of graphene, while C_2 is the interface capacitance due to the existence of the interlayer between the metal electrodes and graphene. Parallel connection of the impedances of the low and high conductivity phases is connected in series with the resistance of the metal electrodes and connecting wires to the measurement device (R_e), as well as charge transfer resistances between the electrodes and low/high conductivity mediums (R_{ct1} and R_{ct2}, respectively). The electrical circuit shown in Fig. 5(b) is equivalent to the simplified circuit shown in Fig. 6(a), where the series resistance $R_s = 2(R_e + R_{ct1}R_{ct2}/(R_{ct1} + R_{ct2}))$. The Nyquist plot of the circuit impedance is shown in Fig. 6(b) and

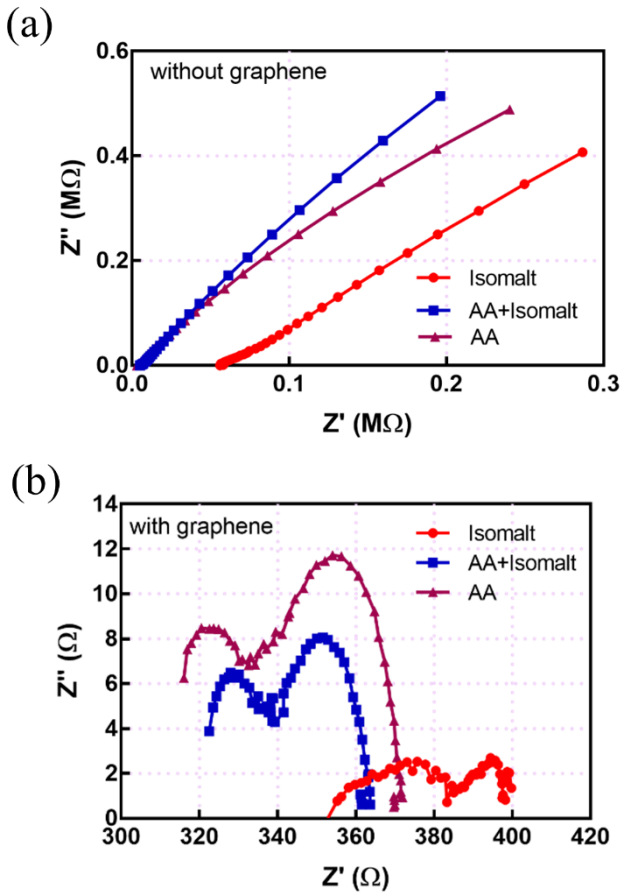

Fig. 7. Nyquist plots for the platform (a) without graphene and (b) with graphene.

it exhibits two semicircles, as theoretically expected. The plot of the same impedance versus frequency is shown in Fig. 6(c). The measured Fig. 3(b) is very similar to Fig. 6(c).

Fig. 7(a) shows Nyquist plots of the measured impedances of the platform without graphene. However, the Nyquist plots for AA (blue line) and 50 % AA + 50 % isomalt (dark magenta) intersect and overlap at low to moderate frequencies making distinction between these two cases difficult. This suggests that higher operating frequencies are required, which can be expensive for in-situ applications.

Fig. 7(b) shows the Nyquist plots of the measured impedances of the platform with graphene. The presence of two semicircles suggests the existence of two materials with different electrical properties which confirms the discussed model.

We used MEISP software tool to fit measured values. The estimated values of the model parameters are shown in Table II.

The quality of the proposed model was estimated by calculating root-mean-square errors (RMSEs) for the real and imaginary part of the complex impedance of the microfluidic platform. Table III shows that RMSEs of the real and imaginary parts of the impedance are $<10\ \Omega$, which is satisfactory considering that the overall order of impedance magnitudes were hundreds of ohms (Fig. 7).

TABLE II
ESTIMATED VALUES OF PARAMETERS OF THE EQUIVALENT ELECTRICAL CIRCUIT SHOWN IN FIG. 6(a)

Fluid	R_s (Ω)	R_1 (Ω)	C_1 (μF)	R_2 (Ω)	C_2 (μF)
Isomalt	362.92	55.15	26.49	33.37	1.47
AA+Isomalt	330.21	27.89	41.17	31.70	4.10
AA	326.91	27.61	41.59	31.38	4.14

TABLE III
RMSE OF THE REAL AND IMAGINARY PART OF THE IMPEDANCE OF THE MICROFLUIDIC PLATFORM WITH GRAPHENE WHEN ISOMALT, ISOMALT + AA, AND AA ARE APPLIED

Fluid	$RMSE_R(\Omega)$	$RMSE_X(\Omega)$
Isomalt	2.74	3.70
AA+Isomalt	2.39	2.23
AA	8.63	3.74

B. Discussion and Description of the Sensing Mechanism

Isomalt ($C_{12}H_{24}O_{11}$) is a mixture of two sugar alcohols: gluco-mannitol and gluco-sorbitol. It has relatively low solubility in water at low temperatures (25 g/100 g at 25 °C) with a high tendency to crystallize [47]. However, AA ($C_6H_8O_6$) is a polar organic molecule that has high water solubility (290 g/L at 20 °C) [48], forming more homogenous structure. AA has 4 hydroxyl groups in its structure providing hydrogen bonds with water molecules and leading to very fast equilibrium and acid nature of the resulting solution after dissolution [49]. The acid nature of AA is recognized from its pH value, which is between 2.4 and 2.8 [50].

Acids ionize (dissociate) in solution, increasing the number of the ions that carry the electric charge, and therefore their presence increases the solution conductivity [51]. From Table II, it can be seen that R_1 is lower for AA in comparison to Isomalt. Moreover, the addition of AA to isomalt reduced R_1 compared to that of pure isomalt. However, C_1 increased, due to the increase of the dielectric constant caused by the reduction of the electric field in the conducting medium, as the concentration of AA is increased. Table II supports this conclusion.

As it was expected, resistance of the graphene layer (R_2) slightly decreased from 33.37 Ω (isomalt) to 31.38 Ω (AA), due to the interaction with AA. Moreover, as the conductivity of graphene is increased, the decrease of the insulating properties of the device leads to the increase of C_2. Table II supports these conclusions, providing additional verification of the presented sensing mechanism and proposed equivalent electrical circuit.

Moreover, it can be noted that series resistance R_s decreases with increased AA concentration. Decrease of R_s provides a main justification for adding graphene. As noted above, R_s is composed of a series connection of the electrode resistances and connecting wires (R_e, which should not change with the concentration of AA) and equivalent resistance of the parallel connection of the charge transfer resistances (R_{ct1} and R_{ct2} in Fig. 5(b)). As graphene layer provides current path of very high conductivity, it has small charge transfer resistance, which

TABLE IV
COMPARISON OF RELATED WORKS AA SENSING

Ref.	Sensing material	Measurement range	Sensed parameters	Readout apparatus
[17]	Serpentine polydimethylsiloxane (PDMS) microchannel is modified by enzyme via physisorption	LOD: 10 μM of AA in the presence of 100 μM caffeine	AA in the presence of caffeine	UV/vis spectroscopy
[18]	Alumina sol-gel encapsulation, physisorption to PDMS channels with, and without alumina xerogel modification	LOD: 2.4±0.1 μM	AA quantification in human blood	UV/vis spectroscopy
[19]	Carbon paste electrodes	0.02 mM – 3.0 mM for DA 0.04 mM – 3.0 mM for AA	AA, dopamine (DA)	Potentiostat
[20]	Paper-based separation devices	0 – 0.4 mmol/L	AA, uric acid (UA)	Amperometric
[21]	Pencil drawn electrochemical paper-based analytical devices	0.5 – 3.0 mmol/L	AA	Cyclic voltammetry (CV) and square wave voltammetry
[22]	Graphite paper electrode	20 – 400 μM for AA 0.5 – 35 μM for DA 0.5 – 35 μM for UA	AA, DA, UA	CV, different pulse voltammetry (DPV) and EIS
[26]	Spherical MOF-5 arrayed on a three-dimensional porous carbon electrode	0.7 μM – 11.5 mM	AA	CV and amperometric
[28]	Glassy carbon electrode modified by carboxyl multi-walled carbon nanotubes	10^{-6} - 10^{-3} mol/L	AA	Electrochemical potentiostat
[29]	Graphene/CuPc/P ANI nanocomposites	100 μM – 3.6 mM	AA	CV
[30]	Hybrid graphene-copper phthalocyanine-polyanilinenanocomposites	5×10^{-7} M – 1.2×10^{-5} M	AA	UV-vis spectroscopy, CV and amperometry
[31]	MBs-AOX/GO/IGZO/Al	0.007 mM – 0.125 mM	L-ascorbic Acid	Potentiometric
[32]	DMF-exfoliated graphene	0.4 mM – 6.0 mM	AA	CV and EIS
[33]	graphene doped carbon paste electrode	1.0×10^{-7} M – 1.06×10^{-4} M	AA	Amperometric, CV, DPV and EIS
[34]	Pristine graphene	9.00 μM –2314μM for AA 5.00 μM –710 μM for DA 6.00 μM –1330 μM for UA	AA, DA, UA	Electrochemical potentiostat and resistivity meter
[35]	Graphene/size-selected Pt nanocomposites	LOD: 0.15μM for AA, 0.03μM for DA, 0.05μM for UA	AA, DA, UA	Amperometric, CV, DPV
[36]	Electro-deposited NiO/graphene composite film modified electrode	0.05 μM to 1100 μM	AA in the presence of folic acid	DPV
This work	Microfluidic channel placed between the silver electrodes with graphene sheet deposited in the gap between the electrodes	Pure isomalt 50% of isomalt + 50% of AA Pure AA	AA in the presence of isomalt	EIS

reduces the resistance of the parallel connection of R_{ct1} and R_{ct2}. Therefore, the addition of graphene layer enhances the electron transfer [52].

The sensing mechanism of the developed microfluidic platform is based on the increase of the overall conductivity with the increase of the concentration of AA, resulting in the decrease of the resistive parameters and increase of the capacitive parameters of the equivalent electrical circuit. The proposed model better fits (lower RMSE values in Table III) the impedance of the microfluidic platform in the presence of isomalt.

C. Performance Comparison of the Proposed Device With the State of the Art

Table IV compares our work to other studies focused on the development of platforms for the precise detection of AA concentration. Considering that commercially available vitamin C supplements also contain a significant amount of sweeteners, it is also crucial to differentiate AA from isomalt, a widely used sugar substitute. Table IV demonstrates a lack of such studies and our study intends to cover this gap.

IV. CONCLUSION

In this study, we presented a compact and robust microfluidic platform for the efficient detection of AA. The proposed platform can be used in the food and dietary supplement industry as well as for authenticity checking of-the-shelf products. Such microfluidic platform, which is based on the measurement of electrical impedance, enables determination of the concentration of supplements, and could be of a significant benefit both from the health and economic standpoint. The availability of the proposed microfluidic device would help the interested parties: consumers - to choose the desired product, pharmacists - to sell only high-quality supplements, and producers - to find the right formulations that enable prolonged shelf-life and by not having to add more than necessary of the active substance into the product.

We provided details regarding design, fabrication and characterization of the microfluidic platform suitable for the detection of AA. The equivalent electrical circuit, based on the theoretical analysis and experimental measurements, was verified. The sensing mechanism and the electrical parameters in the presence of AA in the microfluidic channel were described. We found that our microfluidic platform is capable of differentiating between the solutions comprising pure AA, mixture of AA and isomalt, and pure isomalt.

The future work should be directed to the development and implementation of the device for in-situ impedance measurement with the presented microfluidic platform. Such an approach should reduce the overall cost of the system and processing time from taking a sample to providing information on ascorbic acid presence. Moreover, the determination of serum AA concentrations is frequently performed in medical biochemistry laboratories, usually as a part of automated biochemical analyses. A separate set of experiments should be designed in order to validate the use of our sensor in the clinical setting, investigate possible interference substances otherwise present in the biological materials, and ultimately determine reproducibility and other performance characteristics (i.e., cut-off values) [53]. Our sensor could also be used to validate acetylsalicylic acid in serum, plasma, erhytrocyte hemolisate, and urine. Other biological materials, such as saliva or sweat samples should also be taken into consideration.

REFERENCES

[1] A. Santini and E. Novellino, "Nutraceuticals–shedding light on the grey area between pharmaceuticals and food," *Expert Rev. Clin. Pharmacol.*, vol. 11, no. 6, pp. 545–547, Jun. 2018, doi: 10.1080/17512433.2018.1464911.

[2] J. C. Rickman, D. M. Barrett, and C. M. Bruhn, "Nutritional comparison of fresh, frozen and canned fruits and vegetables. Part 1. Vitamins C and B and phenolic compounds," *J. Sci. Food Agricult.*, vol. 87, no. 6, pp. 930–944, 2007.

[3] I. Klimczak and A. Gliszczyńska-Świgło, "Comparison of UPLC and HPLC methods for determination of vitamin C," *Food Chem.*, vol. 175, pp. 100–105, May 2015.

[4] R. O. Hassan and A. T. Faizullah, "Reverse-FIA with spectrophotometric detection method for determination of vitamin C," *J. Iranian Chem. Soc.*, vol. 8, no. 3, pp. 662–673, Sep. 2011.

[5] T. Maki, N. Soh, K. Nakano, and T. Imato, "Flow injection fluorometric determination of ascorbic acid using perylenebisimide-linked nitroxide," *Talanta*, vol. 85, no. 4, pp. 1730–1733, Sep. 2011.

[6] Z. Gazdik *et al.*, "Determination of vitamin C (ascorbic acid) using high performance liquid chromatography coupled with electrochemical detection," *Sensors*, vol. 8, no. 11, pp. 7097–7112, Nov. 2008, doi: 10.3390/s8117097.

[7] S. Kumar, R. Singh, Q. Yang, S. Cheng, B. Zhang, and B. K. Kaushik, "Highly sensitive, selective and portable sensor probe using germanium-doped photosensitive optical fiber for ascorbic acid detection," *IEEE Sensors J.*, vol. 21, no. 1, pp. 62–70, Jan. 2021, doi: 10.1109/JSEN.2020.2973579.

[8] G. Zhu *et al.*, "A novel periodically tapered structure-based gold nanoparticles and graphene oxide–immobilized optical fiber sensor to detect ascorbic acid," *Opt. Laser Technol.*, vol. 127, Jul. 2020, Art. no. 106156.

[9] L. Hou, Y. Cui, M. Xu, Z. Gao, J. Huang, and D. Tang, "Graphene oxide-labeled sandwich-type impedimetric immunoassay with sensitive enhancement based on enzymatic 4-chloro-1-naphthol oxidation," *Biosensors Bioelectron.*, vol. 47, pp. 56–149, Sep. 2013.

[10] L. Hou, Y. Tang, M. Xu, Z. Gao, and D. Tang, "Tyramine-based enzymatic conjugate repeats for ultrasensitive immunoassay accompanying tyramine signal amplification with enzymatic biocatalytic precipitation," *Anal. Chem.*, vol. 86, no. 16, pp. 8352–8358, Aug. 2014.

[11] L. Hou, X. Wu, G. Chen, H. Yang, M. Lu, and D. Tang, "HCR-stimulated formation of DNAzyme concatamers on gold nanoparticle for ultrasensitive impedimetric immunoassay," *Biosensors Bioelectron.*, vol. 68, pp. 487–493, Jun. 2015.

[12] J. Zhuang, L. Fu, W. Lai, D. Tang, and G. Chen, "Target-stimulated metallic HgS nanostructures on a DNA-based polyion complex membrane for highly efficient impedimetric detection of dissolved hydrogen sulfide," *Chem. Commun.*, vol. 49, no. 95, pp. 11200–11202, 2013.

[13] L. Hou *et al.*, "DNAzyme-functionalized gold–palladium hybrid nanostructures for triple signal amplification of impedimetric immunosensor," *Biosensors Bioelectron.*, vol. 54, pp. 365–371, Apr. 2014.

[14] Z. Qiu, D. Tang, J. Shu, G. Chen, and D. Tang, "Enzyme-triggered formation of enzyme-tyramine concatamers on nanogold-functionalized dendrimer for impedimetric detection of Hg(II) with sensitivity enhancement," *Biosensors Bioelectron.*, vol. 75, pp. 108–115, Jan. 2016.

[15] M. Xu, Z. Gao, Q. Wei, G. Chen, and D. Tang, "Hemin/G-quadruplex-based DNAzyme concatamers for *in situ* amplified impedimetric sensing of copper(II)ion coupling with DNAzyme-catalyzed precipitation strategy," *Biosensors Bioelectron.*, vol. 74, pp. 1–7, Dec. 2015.

[16] N. Nesakumar, S. Kesavan, C.-Z. Li, and S. Alwarappan, "Microfluidic electrochemical devices for biosensing," *J. Anal. Test.*, vol. 3, no. 1, pp. 3–18, Jan. 2019, doi: 10.1007/s41664-019-0083-y.

[17] H. Bi, A. C. Fernandes, S. Cardoso, and P. Freitas, "Interference-blind microfluidic sensor for ascorbic acid determination by UV/vis spectroscopy," *Sens. Actuators B, Chem.*, vol. 224, pp. 668–675, Mar. 2016, doi: 10.1016/j.snb.2015.10.072.

[18] H. Bi, C. M. Duarte, M. Brito, V. Vilas-Boas, S. Cardoso, and P. Freitas, "Performance enhanced UV/vis spectroscopic microfluidic sensor for ascorbic acid quantification in human blood," *Biosensors Bioelectron.*, vol. 85, pp. 568–572, Nov. 2016, doi: 10.1016/j.bios.2016.05.054.

[19] A. Suea-Ngam, P. Rattanarat, O. Chailapakul, and M. Srisa-Art, "Electrochemical droplet-based microfluidics using chip-based carbon paste electrodes for high-throughput analysis in pharmaceutical applications," *Anal. Chim. Acta*, vol. 883, pp. 45–54, Jul. 2015, doi: 10.1016/j.aca.2015.03.008.

[20] R. F. Carvalhal, M. S. Kfouri, M. H. de Oliveira Piazetta, A. L. Gobbi, and L. T. Kubota, "Electrochemical detection in a paper-based separation device," *Anal. Chem.*, vol. 82, no. 3, pp. 1162–1165, Feb. 2010, doi: 10.1021/ac902647r.

[21] V. X. G. Oliveira, A. A. Dias, L. L. Carvalho, T. M. G. Cardoso, F. Colmati, and W. K. T. Coltro, "Determination of ascorbic acid in commercial tablets using pencil drawn electrochemical paper-based analytical devices," *Anal. Sci.*, vol. 34, no. 1, pp. 91–95, 2018, doi: 10.2116/analsci.34.91.

[22] W. Cai, T. Lai, H. Du, and J. Ye, "Electrochemical determination of ascorbic acid, dopamine and uric acid based on an exfoliated graphite paper electrode: A high performance flexible sensor," *Sens. Actuators B, Chem.*, vol. 193, pp. 492–500, Mar. 2014.

[23] G. Cai, Z. Yu, R. Ren, and D. Tang, "Exciton–plasmon interaction between AuNPs/graphene nanohybrids and CdS quantum dots/TiO_2 for photoelectrochemical aptasensing of prostate-specific antigen," *ACS Sensors*, vol. 3, no. 3, pp. 632–639, 2018.

[24] J. Shu, Z. Qiu, and D. Tang, "Self-referenced smartphone imaging for visual screening of H_2S using Cu_x O-polypyrrole conductive aerogel doped with graphene oxide framework," *Anal. Chem.*, vol. 90, no. 16, pp. 9691–9694, 2018.

[25] R. Zeng, Z. Luo, L. Zhang, and D. Tang, "Platinum nanozyme-catalyzed gas generation for pressure-based bioassay using polyaniline nanowires-functionalized graphene oxide framework," *Anal. Chem.*, vol. 90, no. 20, pp. 12299–12306, Oct. 2018.

[26] Y. Song, C. Gong, D. Su, Y. Shen, Y. Song, and L. Wang, "A novel ascorbic acid electrochemical sensor based on spherical MOF-5 arrayed on a three-dimensional porous carbon electrode," *Anal. Methods*, vol. 8, no. 10, p. 2290, 2016, doi: 10.1039/C6AY00136J.

[27] X. Liu *et al.*, "A glassy carbon electrode modified with the nickel(II)-bis(1,10-phebabthroline) complex and multi-walled carbon nanotubes, and its use as a sensor for ascorbic acid," *Microchim. Acta*, vol. 180, pp. 1309–1316, Jul. 2013, doi: 10.1007/s00604-013-1058-8.

[28] B. He and J. Zhang, "Electrochemical determination of vitamin C on glassy carbon electrode modified by carboxyl multi-walled carbon nanotubes," *Int. J. Electrochem. Sci.*, vol. 10, pp. 9621–9631, Nov. 2015.

[29] S. Pakapongpan, J. P. Mensing, T. Lomas, and A. Tuantranont, "Electrochemical sensor for ascorbic acid based on graphene/CuPc/PANI nanocomposites," in *Proc. IEEE Int. Conf. Electron Devices Solid State Circuit (EDSSC)*, Dec. 2012, pp. 1–3, doi: 10.1109/EDSSC.2012.6482864.

[30] S. Pakapongpan, J. P. Mensing, D. Phokharatkul, T. Lomas, and A. Tuantranont, "Highly selective electrochemical sensor for ascorbic acid based on a novel hybrid graphene-copper phthalocyanine-polyaniline nanocomposites," *Electrochim. Acta*, vol. 133, pp. 294–301, Jul. 2014, doi: 10.1016/j.electacta.2014.03.167.
[31] J.-C. Chou *et al.*, "Determination of L-ascorbic acid using MBs-AOX/GO/IGZO/Al by wireless sensing system and microfluidic framework," *IEEE Access*, vol. 7, pp. 45872–45880, 2019.
[32] G. P. Keeley, A. O'Neill, N. McEvoy, N. Peltekis, J. N. Colemanac, and G. S. Duesberg, "Electrochemical ascorbic acid sensor based on DMF-exfoliated graphene," *J. Mater. Chem.*, vol. 20, no. 36, pp. 7864–7869, 2010, doi: 10.1039/C0JM01527J.
[33] F. Li, J. Li, Y. Feng, L. Yang, and Z. Du, "Electrochemical behavior of graphene doped carbon paste electrode and its application for sensitive determination of ascorbic acid," *Sens. Actuators B, Chem.*, vol. 157, no. 1, pp. 110–114, Sep. 2011, doi: 10.1016/j.snb.2011.03.033.
[34] S. Qi, B. Zhao, H. Tang, and X. Jiang, "Determination of ascorbic acid, dopamine, and uric acid by a novel electrochemical sensor based on pristine graphene," *Electrochim. Acta*, vol. 161, pp. 395–402, Apr. 2015, doi: 10.1016/j.electacta.2015.02.116.
[35] C.-L. Sun, H.-H. Lee, J.-M. Yang, and C.-C. Wu, "The simultaneous electrochemical detection of ascorbic acid, dopamine, and uric acid using graphene/size-selected Pt nanocomposites," *Biosensors Bioelectron.*, vol. 26, no. 8, pp. 3450–3455, Apr. 2011, doi: 10.1016/j.bios.2011.01.023.
[36] B. Liu *et al.*, "Differential pulse voltammetric determination of ascorbic acid in the presence of folic acid at electro-deposited NiO/graphene composite film modified electrode," *Electrochim. Acta*, vol. 142, pp. 336–342, Oct. 2014, doi: 10.1016/j.electacta.2014.07.126.
[37] F. Mao, U. Wiklund, A. M. Andersson, and U. Jansson, "Graphene as a lubricant on Ag for electrical contact applications," *J. Mater. Sci.*, vol. 50, no. 19, pp. 6518–6525, Oct. 2015, doi: 10.1007/s10853-015-9212-9.
[38] T. Kojić, G. Stojanović, A. Miletić, M. Radovanović, H. Al-Salami, and F. Arduini, "Testing and characterization of different papers as substrate material for printed electronics and application in humidity sensor," *Sensors Mater.*, vol. 31, no. 9, pp. 2981–2995, 2019.
[39] D. Z. Vasiljevic, A. Mansouri, L. Anzi, R. Sordan, and G. M. Stojanovic, "Performance analysis of flexible ink-jet printed humidity sensors based on graphene oxide," *IEEE Sensors J.*, vol. 18, no. 11, pp. 4378–4383, Jun. 2018.
[40] *PhytoNet AG*. Accessed: Feb. 20, 2021. [Online]. Available: https://phytonet-doo.business.site/
[41] *Syringe Filters*. Accessed: Apr. 10, 2021. [Online]. Available: https://www.sigmaaldrich.com/labware/syringe-filters.html
[42] *Filters for Cell Culture*. Accessed: Apr. 10, 2021. [Online]. Available: https://www.sigmaaldrich.com/technical-documents/articles/biology/sterile-millex-filters-for-cell-culture.html
[43] V. F. Lvovich, *Impedance Spectroscopy: Applications to Electrochemical and Dielectric Phenomena*. Hoboken, NJ, USA: Wiley, 2012, p. 50.
[44] N. O. Weiss *et al.*, "Graphene: An emerging electronic material," *Adv. Mater.*, vol. 24, no. 43, pp. 5782–5825, Nov. 2012.
[45] C. Yim, N. McEvoy, H.-Y. Kim, E. Rezvani, and G. S. Duesberg, "Investigation of the interfaces in Schottky diodes using equivalent circuit models," *ACS Appl. Mater. Interfaces*, vol. 5, no. 15, pp. 6951–6958, Aug. 2013, doi: 10.1021/am400963x.
[46] M. Das *et al.*, "Equivalent circuit analysis of Al/rGO-TiO_2 metal-semiconductor interface via impedance spectroscopy: Graphene induced improvement in carrier mobility and lifetime," *Mater. Sci. Semiconductor Process.*, vol. 82, pp. 104–111, Aug. 2018, doi: 10.1016/j.mssp.2018.03.039.
[47] H. Schiweck *et al.*, "Sugar alcohols," in *Ullmann's Encyclopedia of Industrial Chemistry*. Hoboken, NJ, USA: Wiley, 2000, doi: 10.1002/14356007.a25_413.pub2.
[48] A. N. Soriano, K. G. R. Dollente, R. J. D. Tabaquero, and A. P. Adornado, "Estimation of diffusion coefficients of ascorbate-based ions at infinite dilution through electrolytic conductivity measurements," *IOP Conf. Ser., Earth Environ. Sci.*, vol. 191, Nov. 2018, Art. no. 012028, doi: 10.1088/1755-1315/191/1/012028.
[49] A. C. Ribeiro Neto, R. F. Pires, R. A. Malagoni, and M. R. Franco, "Solubility of vitamin C in water, ethanol, Propan-1-ol, water + ethanol, and water + Propan-1-ol at (298.15 and 308.15) K," *J. Chem. Eng. Data*, vol. 55, no. 4, pp. 1718–1721, Apr. 2010, doi: 10.1021/je900687y.
[50] National Center for Biotechnology Information. *PubChem Compound Summary for CID 54670067, Ascorbic Acid*. Accessed: Feb. 20, 2021. [Online]. Available: https://pubchem.ncbi.nlm.nih.gov/compound/Ascorbic-acid
[51] T. Leveling, "The relationship between pH and conductivity in a lithium contaminated, de-ionized water system," Fermilab Tech. Publications, Batavia, IL, USA, Pbar Note 675, 2002.
[52] A. Kaplan *et al.*, "Current and future directions in electron transfer chemistry of graphene," *Chem. Soc. Rev.*, vol. 46, no. 15, pp. 4530–4571, 2017, doi: 10.1039/c7cs00181a.
[53] S. Kumar *et al.*, "Development of uric acid biosensor using gold nanoparticles and graphene oxide functionalized micro-ball fiber sensor probe," *IEEE Trans. Nanobiosci.*, vol. 19, no. 2, pp. 173–182, Apr. 2020, doi: 10.1109/TNB.2019.2958891.

Goran M. Stojanović (Member, IEEE) received the B.Sc., M.Sc., and Ph.D. degrees in electrical engineering from FTS-UNS in 1996, 2003, and 2005, respectively. He is a Full Professor with the Faculty of Technical Sciences (FTS), University of Novi Sad (UNS), Serbia. He has 25 years of experience in research and development. He is an author/coauthor of 260 articles, including 96 in leading peer-reviewed journals with impact factors, five books, three patents, one chapter in monograph. He was a Keynote Speaker for 12 international conferences. He has been a Supervisor of 11 Ph.D. students, 40 M.Sc. students, and 60 Diploma students with FTS-UNS. He has more than 14 years' experience in coordination of EU funded projects (H2020, FP7, EUREKA, ERASMUS, and CEI), with total budget exceeding 14.86 MEUR. He currently coordinates four Horizon2020 projects in the field of green electronics and textile electronics. His research interests include sensors, flexible electronics, textile electronics, and microfluidics.

Tijana Kojić received the B.Sc. and M.Sc. degrees in electrical engineering from the Faculty of Technical Science, University of Novi Sad, Serbia, in 2013 and 2015, respectively, where she is currently pursuing the Ph.D. degree. She is mainly involved in designing and fabrication of flexible/organic/printed sensors and nanomaterials characterization appropriate for sensing applications. The main focus of her research are innovative and flexible paper-based electronics.

Mitar Simić (Member, IEEE) was born in Ljubovija, Serbia, in 1987. He received the B.Sc. and M.Sc. degrees in electrical engineering from the University of East Sarajevo, Bosnia and Herzegovina, in 2010 and 2012, respectively, and the Ph.D. degree in electrical engineering from the University of Novi Sad, Serbia, in 2017. He is a Postdoctoral Researcher with the STRENTEX Project, Faculty of Technical Sciences, University of Novi Sad, Serbia. He is an author/coauthor of one monograph and more than 40 scientific articles. His research interests include sensors, flexible electronics, impedance spectroscopy analysis, equivalent circuit modeling, and development of devices for impedance measurement, and data acquisition.

Aleksandra Jovanović-Galović received the B.Sc. degree in biology and the Ph.D. degree in biochemistry from the Faculty of Natural Sciences, University of Novi Sad. She has done her postdoctoral studies with the Faculty of Medicine, University of Padua, Italy. She worked as a Visiting Research Scientist with the Office of Medical Examiner of the City of New York, USA. She was as an Associate Professor with the Faculty of Pharmacy Novi Sad, Serbia, where she is currently teaching general and medical biochemistry, immunochemistry and immunology. Her scientific interests include multidiciplinary research, at the intersection of biology, chemistry, and physics.

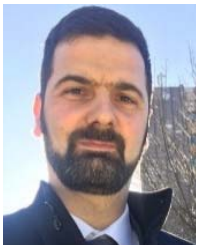

Bojan Pavlović received the Ph.D. degree in pharmaceutical sciences from the University of Belgrade, Serbia. He had a career that combined technical expertise and marketing skills in new dietary supplement product design and development, new business development, in licensing, out licensing, and sales of scientifically proven dietary supplements for the territory of southern and eastern Europe. He is actively involved in intellectual property management, market research and designing and execution of business plans, preparation of quality assurance documentation for research and development pharma projects, and manufacturing and launching of new products. He is currently the Chief Executive Officer with PhytoNet AG company, Novi Sad, Serbia.

Amaia Zurutuza received the Ph.D. degree in polymer chemistry from the University of Strathclyde, Glasgow, U.K., in 2002. From 2001 to 2003, she was a Postdoctoral Research Fellow working in two European projects related to molecularly imprinted polymers. In 2004, she joined Ferring Pharmaceuticals (previously Controlled Therapeutics), where she worked in the research of new controlled drug delivery systems as a Senior Polymer Scientist. Her contribution led to the granting of three patents in novel biodegradable and biostable polymers for the controlled release of active compounds. In 2010, she became the Scientific Director of Graphenea. At Graphenea, she leads the research and development activities on graphene-based materials. Since joining Graphenea, she has been so far filed for 12 patents and published more than 74 publications in peer reviewed journals, including nature and science. She was a principal investigator of 21 EU FP7/H2020 funded research projects, 16 collaborative projects, including the Graphene Flagship, and three people training network projects. In the Graphene Flagship, she is a member of the Executive Board and the World Package Deputy Leader of the wafer scale integration (Graphene Flagship) and wafer scale growth (Experimental Pilot Line) work packages. In addition, she has also given more than 52 invited talks in international conferences. Her research interests include the synthesis, characterization, and future industrial applications of graphene.

Luca Anzi was born in Italy, in 1988. He received the B.E. degree in computer science engineering, the M.Sc. degree in materials engineering and nanotechnology, and the Ph.D. in physics from the Polytechnic University of Milan, Italy, in 2011, 2014, and 2018, respectively. Since 2018, he has been a Postdoctoral Research Fellow with the Department of Physics, Polytechnic University of Milan, Italy. His main area of research interest includes the use of graphene among other 2D materials for nanoelectronic devices and circuits.

Roman Sordan received the Ph.D. degree in solid state physics from the University of Belgrade, Serbia, in 1999. He is an Associate Professor of Physics with the Polytechnic University of Milan, Italy. He was previously with the Max Planck Institute for Solid State Research in Stuttgart, Germany. He is currently a Principal Investigator with Graphene Flagship Project. His current research interests include the integration of graphene and other two-dimensional materials in nanoelectronic devices and circuits.